Accepted Manuscript

Water transfer in bread during staling: Physical phenomena and modelling

Jean-Yves Monteau, Emmanuel Purlis, Emna Besbes, Vanessa Jury, Alain Le-Bail

PII: S0260-8774(17)30152-8

DOI: 10.1016/j.jfoodeng.2017.04.016

Reference: JFOE 8851

To appear in: *Journal of Food Engineering*

Received Date: 12 September 2016

Revised Date: 8 March 2017

Accepted Date: 8 April 2017

Please cite this article as: Monteau, J.-Y., Purlis, E., Besbes, E., Jury, V., Le-Bail, A., Water transfer in bread during staling: Physical phenomena and modelling, *Journal of Food Engineering* (2017), doi: 10.1016/j.jfoodeng.2017.04.016.

Water transfer in bread during staling: physical phenomena and modelling

Jean-Yves Monteau[a,b,*], Emmanuel Purlis[a,b,c], Emna Besbes[a,b], Vanessa Jury[a,b], Alain Le-Bail[a,b]

[a] *UBL, Oniris, département GPA, rue de la Géraudière, B.P. 82 225 44322 Nantes CEDEX 3, France*
[b] *GEPEA UMR CNRS 6144, Nantes, France*
[c] *Centro de Investigación y Desarrollo en Criotecnología de Alimentos (CIDCA), UNLP, CONICET, Facultad de Ciencias Exactas, 47 y 116, La Plata (1900), Argentina*

Abstract

Starch retrogradation and water loss have effects of the same intensity on the increase in firmness in the phenomenon of bread staling. Writing the equations of this system, in order to understand the mechanisms of water transfer in the vapour and liquid phases, is apparently simple. Nevertheless, choices are necessary for the simplifying hypotheses. Two models, differing in their geometry and their equations, were developed. Besides investigating the water transfer mechanisms in the vapour and liquid phases, the aim of this study is to compare the results of the two models and to conclude as to their individual interest. Concerning the physical phenomena, the study shows that a part of the water lost by the crumb escapes into the atmosphere while another part is absorbed by the crust. As regards the modelling the study shows that the most complete model is not the best choice and specifies the simplifying assumptions that should be retained or eliminated.

*Corresponding author
Email address: jean-yves.monteau@oniris-nantes.fr (Jean-Yves Monteau)

Keywords: Sandwich bread, staling, water transfer modelling

1. Introduction

The staling of bread is defined as its firming over time and results in a loss of smoothness (Roussel and Chiron, 2002). Not only are its textural properties modified but also its aromatic properties. This evolution is perceptible for a product like sandwich bread sold in a tight packaging. The retrogradation of starch is essential for staling (Hug-Iten et al., 1999), but water migration plays an important part through its distribution among the bread components. In fact, bread with crust loses its freshness quickly while bread without crust stays fresh (Bechtel et al., 1953; Besbes et al., 2014). However, the effect of the presence of the crust is exerted on the exchange of water between the crumb, the crust and the atmosphere and not on starch retrogradation. According to Ronda et al. (2011), starch retrogradation and water loss have effects of the same intensity on the increase in bread firming. Water migration results in an equilibration of the water content between the crust and the crumb at the macroscopic scale and in the redistribution of moisture between the components at the microscopic scale. This equilibrium is unstable and may drift towards crust softening and crumb drying.

Water transfer in a product is driven by different mechanisms: molecular diffusion (gas phase), convection and liquid capillarity. Several authors have used a simple model based on molecular diffusion in dense, homogeneous and isotropic media with Fick's second law to describe the mass transfer (Datta, 2005). However, the mass transfer of water in liquid or in vapour form was

not differentiated. Other authors, for instance Thorvaldsson and Janestad (1999), preferred to use Fick's law in separating liquid water transfer and water vapour transfer. Nevertheless, Fick's law alone does not explain the mass transfer in porous media because diffusion is not the only mechanism responsible. Therefore, it is necessary to add a convection term to the diffusion term based on Darcy's law: the transfer is then also due to a pressure gradient. A synthesis of formulations of heat and mass transfer problems has been provided by Datta (2007a).

To understand the mechanisms of water transfer in bread during staling, we have developed models of the system. Modelling a process involves a number of assumptions and choices for the equations. Thus the same process can be described by several models, with the most complex in terms of its equations not necessarily being the best. For bread staling we tested two models with the following main assumptions, respectively: constant pressure and incorporation of the crust via the water vapour permeability in the boundary conditions; a composite domain (crumb and crust) with variable pressure. The aim of this work is to compare the results given by these two models and to conclude about their application scope.

2. Modelling

The modelling is greatly inspired by the model of Whitaker (1977) developed for the drying process, with some adaptations to the staling problem. The problem is isothermal. So, there is no heat transfer equation. We are particularly interested in three quantities varying in time and 2D-space: the

local content of liquid water, water vapour and dry air, these two gases forming the gaseous phase. The geometry is the upper right quarter of a slice of bread, placed horizontally in order to eliminate the gravitational effect (Figure 1). For the first model, the crust is assumed to be a membrane characterised by its water vapour permeability.

In the first model, the pressure of the bread slice is assumed equal to atmospheric pressure. The system modelling is based on two governing equations: one for liquid water and one for the local water vapour content. Because the total pressure is constant, the dry air pressure and the local dry air content are derived from the local water vapour content.

In the second model, the crust is a domain with its own characteristics (density, porosity, etc.) different from the crumb. The total pressure is no longer supposed constant. The local dry air content is assumed to be governed by a similar equation to that which governs the local water vapour content. Partial pressures of each gas and thus the total pressure can vary.

Figure 1 presents a summary of assumptions of each model, which are further discussed next.

2.1. First Model

The variation in the local water content, X_{liq}, is described by Darcy flow (due to liquid pressure: $P_{\mathrm{liq}} = P - P_{\mathrm{c}}$) with the addition of an evaporation-

condensation volumetric rate, I:

$$\frac{\partial X_{\text{liq}}}{\partial t} = \nabla \cdot \left[\rho_{\text{liq}} \frac{k_{\text{liq}}}{\mu_{\text{liq}}} \nabla \left(P - P_{\text{c}} \right) \right] - I \tag{1}$$

where P_{c} is the capillary pressure and P the total pressure. ρ_{liq} and μ_{liq} are the density and the dynamic viscosity of liquid water, and k_{liq} is the crumb permeability to liquid water. Since liquid water is strongly bound to starch, the total pressure of the driven flow is not significant in our case, so the following expression is used:

$$\frac{\partial X_{\text{liq}}}{\partial t} = \nabla \cdot \left(D_{\text{liq}} \nabla X_{\text{liq}} \right) - I \tag{2}$$

where D_{liq} is the capillary diffusivity of liquid water, defined as (Datta, 2007b):

$$D_{\text{liq}} = -\rho_{\text{liq}} \frac{k_{\text{liq}}}{\mu_{\text{liq}}} \frac{\partial P_{\text{c}}}{\partial X_{\text{liq}}} \tag{3}$$

The variation in water vapour, X_{vap}, is driven by a diffusion equation with the corresponding source term:

$$\frac{\partial X_{\text{vap}}}{\partial t} = \nabla \cdot \left[\rho_{\text{g}} \Phi \left(1 - S \right) D_{\text{av}} \nabla \frac{\rho_{\text{vap}}}{\rho_{\text{g}}} \right] + I \tag{4}$$

The air-vapour diffusion coefficient D_{av} is weighted by the ratio of gas volume to total volume, i.e. the porosity Φ multiplied by the gas fraction in the pores, $1 - S$; S is the water saturation in the pores and ρ_{g} is the gas density.

The evaporation-condensation rate is assumed proportional to the difference between the equilibrium water vapour pressure, $a_w \, P_{\text{sat}}(T)$, and the vapour pressure in the pores P_{vap}. a_w is the crumb water activity and $P_{\text{sat}}(T)$ is the saturation pressure of the water vapour at temperature T:

$$I = C \left[a_w \, P_{\text{sat}}(T) - P_{\text{vap}} \right] \tag{5}$$

C is the proportionality coefficient. The crumb water activity was experimentally determined to fill a table function of the local water content (Besbes et al., 2013). This table is interpolated using piecewise cubic functions. The water vapour pressure is derived from the perfect gas law:

$$P_{\text{vap}} = \frac{X_{\text{vap}}\, R\, T}{M_{\text{vap}}\, \Phi\, (1 - S)} \tag{6}$$

where R is the perfect gas law constant and M_{vap} is the molar mass of water vapour.

This first model is characterised by a total pressure assumed constant and equal to atmospheric pressure. Thus, the dry air pressure is derived by subtracting the water vapour pressure from the total pressure:

$$P_{\text{air}} = P - P_{\text{vap}} \tag{7}$$

Then, the dry air content X_{air} is derived using the perfect gas law:

$$X_{\text{air}} = \frac{P_{\text{air}}\, M_{\text{air}}\, \Phi\, (1 - S)}{R\, T} \tag{8}$$

where M_{air} is the molar mass of dry air.

The water vapour and dry air densities can be calculated from the mass concentrations in the porous matrix:

$$\rho_{\text{vap}} = \frac{X_{\text{vap}}}{\Phi\, (1 - S)} \tag{9}$$

$$\rho_{\text{air}} = \frac{X_{\text{air}}}{\Phi\, (1 - S)} \tag{10}$$

The saturation pressure is calculated with the Dupré formula, which can be used from -50 to 200 ℃:

$$P_{\text{sat}}(T) = 133.32 \exp(46.784 - \frac{6435}{T} - 3.868 \ln T) \tag{11}$$

where T is in K and P_{sat} in Pa. The problem is isothermal, thus P_{sat} is constant.

The pores saturation is calculated with the following equation:

$$S = \frac{X_{\text{liq}}}{\rho_{\text{liq}} \Phi} \tag{12}$$

Lastly, the gas density is the sum of the dry air and water vapour densities:

$$\rho_{\text{g}} = \rho_{\text{vap}} + \rho_{\text{air}} \tag{13}$$

2.1.1. Boundary conditions:

The mass transfer with the ambient air is assumed to occur only in the gaseous phase. Consequently, the liquid water flow at the surface is equal to zero, as well as at the left and bottom boundaries because of the symmetries (see Figure 1 a). Thus, in all boundaries, the boundary condition for liquid water is

$$n \cdot (D_{\text{liq}} \nabla X_{\text{liq}}) = 0 \tag{14}$$

where n is the outward normal to the boundary. Regarding X_{vap}, on the left and bottom boundaries, the vapour flow is equal to zero,

$$n \cdot \left[\rho_{\text{g}} \Phi (1 - S) D_{\text{av}} \nabla \frac{\rho_{\text{vap}}}{\rho_{\text{g}}} \right] = 0 \tag{15}$$

and at the surface it is determined by the water vapour permeability of the crust WVP:

$$n \cdot \left[\rho_{\mathrm{g}} \, \Phi \, (1 - S) \, D_{\mathrm{av}} \, \nabla \, \frac{\rho_{\mathrm{vap}}}{\rho_{\mathrm{g}}} \right] = \mathrm{WVP} \, \frac{P_{\mathrm{vap,a}} - P_{\mathrm{vap}}}{e} \tag{16}$$

where e is the crust thickness. The vapour pressure in the ambient air is calculated conventionally by

$$P_{\mathrm{vap,a}} = RH \, P_{\mathrm{sat}}(T) \tag{17}$$

where RH is the ambient relative humidity.

2.2. Second Model

For the second model, the presence of the crust is explicitly incorporated. An external layer (5 mm in thickness) is added to the crumb (Figure 1 b) to represent the crumb-crust composite system. Furthermore, the crumb and crust have different properties, mainly due to differences in structure developed during baking. For instance, the following expressions inspired from (Datta, 2007b) and fitted to our product were used for the capillary diffusivity of liquid water:

$$D_{\mathrm{liq,crumb}} = 1.5 \times 10^{-9} \, e^{(-2.8+2 \, X_{\mathrm{dm}})} \, \Phi \tag{18}$$

$$D_{\mathrm{liq,crust}} = 1 \times 10^{-9} \, e^{(-2.8+2 \, X_{\mathrm{dm}})} \, \Phi \tag{19}$$

where X_{dm} is the local water content on a dry basis. The relationship between X_{liq} and X_{dm} is

$$X_{\mathrm{dm}} = \frac{X_{\mathrm{liq}}}{\rho_{\mathrm{app,dm}}} \tag{20}$$

where $\rho_{\mathrm{app,dm}}$ is the apparent density of the desiccated matrix.

Regarding the water activity of the crust, a water sorption isotherm obtained at 15 ℃ is used (Besbes et al., 2013).

The total pressure a priori can vary, thus the governing equation (1) for the water vapour content is modified by the addition of a flow term.

$$\frac{\partial X_{\mathrm{vap}}}{\partial t} = \nabla \cdot \left[\rho_{\mathrm{g}} \Phi (1 - S) D_{\mathrm{av}} \nabla \frac{\rho_{\mathrm{vap}}}{\rho_{\mathrm{g}}} + \rho_{\mathrm{vap}} \frac{K_{\mathrm{g}}}{\mu_{\mathrm{g}}} \nabla P \right] + I \tag{21}$$

where K_{g} is the permeability of the media to the gaseous phase and μ_{g} the dynamic viscosity of this phase.

K_{g} is given by Equation (22) (Jury, 2007):

$$K_{\mathrm{g}} = 6.55 \times 10^{-11} \Phi^{3.03} \tag{22}$$

μ_{g} is taken equal to air dynamic viscosity (Table 1).

X_{air} is assumed to vary according to a governing equation similar to that governing the evolution of X_{vap}, but without the evaporation-condensation term:

$$\frac{\partial X_{\mathrm{air}}}{\partial t} = \nabla \cdot \left[\rho_{\mathrm{g}} \Phi (1 - S) D_{\mathrm{av}} \nabla \frac{\rho_{\mathrm{air}}}{\rho_{\mathrm{g}}} + \rho_{\mathrm{air}} \frac{K_{\mathrm{g}}}{\mu_{\mathrm{g}}} \nabla P \right] \tag{23}$$

Other equations are unchanged, except for the total pressure P which is no longer equal to atmospheric pressure. From a mathematical point of view, Equation (23) replaces the equation $P = P_{\mathrm{atm}}$, where P_{atm} refers to the atmospheric pressure.

2.2.1. Boundary conditions

For X_{liq}, the boundary conditions are insulation conditions on all the external boundaries, and at the crumb-crust interface there is continuity of the water content. The addition of a partial derivative equation to calculate the dry air content involves defining the boundary conditions for this variable. For the left and bottom boundaries (Figure 1 b) symmetry conditions or zero flow conditions apply. For the surface boundary, a Dirichlet condition, thus a value of the dry air content, cannot be fixed because this value is unknown. In fact, there may be a discontinuity in the dry air content at this boundary. A Neumann condition, i.e. a flow condition, cannot be used because it is not better known. The natural boundary condition is total pressure equal to atmospheric pressure, assuming that it varies without discontinuity from the crumb to the atmosphere. However, a boundary condition for the dry air content cannot be deduced from this pressure condition because the conditions above lead to a Dirichlet condition involving the water vapour content on this boundary. Yet, this Dirichlet condition is not known. Because of this technical difficulty, equations were rewritten to use, as dependent variables, the liquid water and water vapour contents, and the total pressure. The following pressure equation, as governing equation, is thus obtained:

$$\frac{1}{RT}\left(\Phi-\frac{X_{\mathrm{liq}}}{\rho_{\mathrm{liq}}}\right)\frac{\partial P}{\partial t}+\nabla\cdot\left[-\rho_{\mathrm{g}}\,\Phi\,(1-S)\,D_{\mathrm{av}}\left(\frac{1}{M_{\mathrm{vap}}}\nabla\frac{\rho_{\mathrm{vap}}}{\rho_{\mathrm{g}}}+\frac{1}{M_{\mathrm{air}}}\nabla\frac{\rho_{\mathrm{air}}}{\rho_{\mathrm{g}}}\right)-\left(\frac{\rho_{\mathrm{vap}}}{M_{\mathrm{vap}}}+\frac{\rho_{\mathrm{air}}}{M_{\mathrm{air}}}\right)\frac{K_{\mathrm{g}}}{\mu_{\mathrm{g}}}\nabla P\right]=\frac{1}{\rho_{\mathrm{liq}}\,\Phi-X_{\mathrm{liq}}}\left(\frac{X_{\mathrm{vap}}}{M_{\mathrm{vap}}}+\frac{X_{\mathrm{air}}}{M_{\mathrm{air}}}\right)\left[\nabla\cdot\left(D_{\mathrm{liq}}\,\nabla\,X_{\mathrm{liq}}\right)-I\right]+\frac{I}{M_{\mathrm{vap}}}\quad(24)$$

For P, there are symmetry conditions on the left and bottom boundaries, and the Dirichlet condition $P = P_{\text{atm}}$ at the surface. There is pressure continuity at the interface.

For X_{vap}, the same symmetry conditions apply on the left and bottom boundaries as for model 1, and the flow condition (16) is applied at the crumb-crust interface. A boundary condition is necessary at the external surface in contact with the atmosphere. The same difficulties appear as for the air content boundary condition: the water vapour content and the flow of water vapour are unknown at the crust surface. To close the system of equations, the vapour pressure at the surface is assumed equal to that of the atmosphere, which leads to the following Dirichlet condition:

$$X_{\text{vap}} = \frac{P_{\text{vap,a}}\, M_{\text{vap}}\, \Phi\, (1 - S)}{R\, T} \tag{25}$$

2.3. Parameters

The models constants are either known physical constants (D_{av}, R, M_{vap}, etc.), values specific to our product (D_{liq}, Φ, WVP, etc.), or environmental parameters T, P_{atm} and RH. They are given in Table 1. Except for the parameter C, the characteristic values of the product were measured, as were the environmental parameters. The material and methods used and the experimental results are described in (Besbes, 2012).

2.4. Initial conditions

For the first model, the initial conditions necessary to solve the two differential equations were:

$$X_{\text{liq}} = 160\,\text{kg}\,\text{m}^{-3} \quad (X_{\text{dm}} = 0.83) \tag{26}$$

$$X_{\text{vap}} = 7.849 \times 10^{-3}\,\text{kg}\,\text{m}^{-3} \tag{27}$$

The initial liquid water content was set at the experimental value and the water vapour content was determined to be equal to that of the atmosphere.

For the second model, the initial condition necessary to solve Equation (24) was added:

$$P = P_{\text{atm}} \tag{28}$$

For this model, initial conditions for the crust are also necessary. As for the first model X_{liq} was set equal to the experimental value and X_{vap} equal to that of the atmosphere.

$$X_{\text{liq}} = 75.9\,\text{kg}\,\text{m}^{-3} \quad (X_{\text{dm}} = 0.23) \tag{29}$$

$$X_{\text{vap}} = 7.756 \times 10^{-3}\,\text{kg}\,\text{m}^{-3} \tag{30}$$

$$P = P_{\text{atm}} \tag{31}$$

2.5. Programming, geometry and mesh

Programming was achieved using Comsol 4.2 and 4.3. The geometry used the symmetries of the product: a quarter of a bread slice was drawn. The mesh for model 2 was refined until the results at the selected points no longer changed. For model 1 a coarser mesh was sufficient but the same level of refining as for the second model was kept. Meshes are shown in Figure 2.

3. Model fitting

The second model is assumed to be the most realistic as it considers the real geometry with the crust as a distinct area with its own physical characteristics. Besides, it uses the most complete equations without hypotheses about the pressure inside, calculating the dry air content in the same way as the water vapour content and with the flow term. For these reasons, it was selected as the model to best-fit (i.e. fine-tune) the unknown model parameter (namely, the evaporation coefficient) against experimental results.

For the fitting, experimental and computed local water contents averaged on discs were compared. These discs are shown in Figure 2. This resulted in a modification of the mesh. All the discs are in the crumb. In order to obtain water content profiles, averages of the values obtained for a given x-coordinate, or on the height of the slice, were calculated for 4 values of staling time. These values were 2 h (D0), 3 days (D3), 7 days (D7) and 10 days (D10).

The evaporation coefficient C cannot be experimentally determined. C was used as a fitting parameter to fine-tune the numerically simulated water content profiles against experimental counterparts. The value obtained for C is $5 \times 10^{-4}\,\mathrm{s\,m^{-2}}$. Figure 3 illustrates the quality of the fit. The model underestimates the water loss at the start of staling (D0) because the computed water content profile, being constant and nearly equal to the initial value, is above the experimental profile. The profiles computed at D3, D7 and D10 are relatively close to the experimental ones except for the averages

at $x = 38\,\mathrm{mm}$ for the profiles D3 and D7. For these two cases, the computed values are significantly over estimated. However, it is not possible to obtain a better fit with this model, which has only one fitting parameter.

4. Results

4.1. Time variation of the main variables

The analysis in this section is performed on the results given by the 2nd model because it is a priori the most faithful to reality. The local water content is given on a dry basis, X_{dm}, according to the use in food process engineering.

Figure 4 shows the variation in the liquid water content at the different points considered. In the crumb, the local water content decreases constantly. For the inner points, this decrease is linear, starting at point (25, 25) as expected due to its proximity to crust. Note that the centre of the product (point (0, 0)) also shows this trend, which may be due to evaporation since gradients are not significant at the beginning of the process. Underneath the crumb-crust interface (point (34.9, 34.9)), the local water content decreases rapidly during the first day and then very slowly, once initial dehydration due to proximity to crust is diminished and thus the driving force for transport is reduced. On the other hand, above the interface (point (35.1, 35.1)), liquid water content increases rapidly during the first day, but then decreases very slowly. At the midpoint of the crust (point (37, 37)) and surface, liquid water content increases constantly.

These results are explained by a reequilibration of water from the crumb

to the crust, with a decrease at the crumb-crust interface to supply the crust. This rebalancing has already been observed experimentally (Besbes et al., 2014). Above the interface, the increase in the water content at the beginning is also explained by water vapour condensation (see Figure 7). Then, although there is still condensation, the water content decreases. This means that the liquid water diffusion overtakes the condensation. There is a sharp drop in the water content at the crumb-crust interface, although a continuity condition for the water content on a wet basis is imposed. This discontinuity is normal on a dry basis because the relationship between the water content on a wet basis and the water content on a dry basis is given by Equation (20), with $\rho_{\mathrm{app,dm}}$ being different for the crumb and the crust. However, this discontinuity is present on a wet basis despite the continuity boundary condition. In fact, the software complies with the condition but the computation shows that the water content decreases drastically on passing the boundary.

In the crumb the water vapour content increases linearly but the three lines at points (0, 0), (15, 15) and (25, 25) are almost parallel instead of diverging as for the liquid water content (Figure 5). Below the crumb-crust interface, the water vapour content increases rapidly during the first day and afterwards more slowly. Above the interface (point (35.1, 35.1)), it decreases rapidly during day 1, but then rises slowly after 1.6 days. The two curves at the interface end by merging asymptotically. Both the crust and surface points show a similar trend for the water vapour content, which decreases continuously with different rates. Overall, the water vapour content is higher

in the crust than in the crumb until days 6-7; afterwards, the trend is the opposite.

In the crumb, the linear and parallel increase in the water vapour content at the three points considered can be explained by the combination of evaporation and diffusion. Evaporation is almost constant over time for these three points, although with different values (see Figure 7): the closer to the interface, the greater the evaporation. If there was only evaporation, the lines should diverge. A result of this simulation is that the total pressure is constant in the product (Figure 10). Thus, the only driving terms for the movement of the water vapour are evaporation and diffusion, not pressure gradient. Below the interface, the water vapour content increases because of evaporation. In the crumb, the vapour diffusion goes from the centre towards the interface because the water vapour content gradient is oriented inwards. However, at the interface it goes from the crust to the crumb. In the end, the two interface curves (at points (34.9, 34.9) and (35.1, 35.1)) merge and the water vapour content in the crumb becomes higher than that in the crust, because there is still condensation in the crust and evaporation in the crumb (Figure 7).

The dry air content increases linearly in the crumb and faster close to the interface (Figure 6). Below the interface, it first increases rapidly and then more slowly while above it first decreases rapidly before increasing slowly. In the crust and at the surface, it decreases more and more slowly.

The dry air and liquid water contents behave inversely. In the crumb,

the air content increases because the liquid water content decreases, thus decreasing the water saturation of pores. The dry air takes the place released by liquid water. Overall, the dry air content shows the same behaviour as the gas saturation.

In the crumb, the evaporation flow is constant over time but not in space (Figure 7). It is lower at the centre and increases toward the interface. Below the interface, it is initially significant and decreasing exponentially while above the interface it is negative. Thus there is condensation. At the beginning, it rapidly approaches 0, and then decreases very slowly (the condensation increases). In the crust and at the surface, the evaporation flow increases slowly (the condensation decreases).

The evaporation flow results from an imbalance between the terms $a_w\, P_{\text{sat}}$ and P_{vap}, the water vapour pressure (Equation 5). Logically, until the balance is reached, the evaporation flow does not vanish. At the end of the simulation the steady state is still not reached and the condensation continues to decrease at the surface and in the crust. Over time there would probably be a balance, $a_w\, P_{\text{sat}} = P_{\text{vap}}$, but different for the crumb and the crust because the isotherm is not the same for these two areas. The evaporation flow would be zero everywhere but the shelf-life of the product would be greatly exceeded.

In the equations, the water saturation differs from the liquid water content only by a coefficient. The variations are thus similar for the two variables

(Figure 8).

Figure 9 shows the variation in the overall water content for a 1 cm-bread slice in the crumb, the crust and the whole slice.

In the whole slice and the crumb, the water content decreases in two almost parallel lines. However, the water content in the crust increases very slightly in the first two days of staling and then tends to stabilise.

Thus the water that migrates to the atmosphere comes from the crumb, passing by and slightly moistening the crust.

Figure 10 compares the water vapour pressure and dry air pressure in the slice along an axis from the centre to the surface at the end of the simulation (10.2 days). The water vapour pressure in the slice is very low compared to the air pressure. Vapour pressure and air pressure seem constant in the whole product. In reality, for these two gases there is a difference in pressure between the crumb and the crust but due to the y-scale these differences cannot be seen on the figure. The total pressure, although calculated, stays constant and equal to atmospheric pressure. It is a realistic hypothesis that can be used when writing the model equations. An interesting consequence is that there is no Darcy flow because there is no total pressure gradient. Gas transfers only occur by diffusion and evaporation-condensation. The flow terms computed in the equations are found equal to zero.

To resume, these simulation results show that throughout staling there is evaporation in the crumb and condensation in the crust, with water transfer from the crumb to the crust. This results in water loss for the crumb and a gain for the crust, and that overall the bread loses water.

4.2. Comparison of the two models

In the first model, the water vapour content is calculated with a diffusion equation, the total pressure is fixed equal to atmospheric pressure, and the dry air content is deduced. In the second model, the water vapour and the dry air content are calculated in the same way, using a diffusion equation. The crust is considered to be a 5 mm-thick area. The equations are the same as in the crumb but the physical properties differ.

Figures 11 to 15 enable a comparison of the results given by the two models for the crumb (as the crust is represented only by a limit and a boundary condition for the first model, it cannot be used for a comparison). The results are taken at the point (0, 0), the centre of the crumb, and at (34.9, 34.9) just below the crumb-crust interface.

In Figure 11, the comparison of the two models reveals significant differences. The first model overestimates the local water content compared to the second.

Similarly, the first model overestimates the water vapour content compared to the second, either at the centre or below the crumb-crust interface (Figure 12).

Conversely, model 1 underestimates the dry air content compared to model 2 (Figure 13) which is expected as dry air and liquid water contents behave inversely.

The evaporation flow is underestimated by the first model (Figure 14).

The water loss of the crumb given by model 1 is lower than that given by model 2 (Figure 15).

In summary, model 1 overestimates the liquid water and water vapour contents, and underestimates the evaporation flow and the water loss of the crumb compared to model 2. These results show the importance of the water transfer from the crumb to the crust, which cannot be calculated with the first model.

It is worth noting that the model 2, more realistic, based on physical mechanisms (in contrast with purely empirical or semi-empirical models, e.g. using an effective diffusion coefficient that involves several mechanisms) gives us the chance to couple transport models with quality models, for example, to predict rheological properties related to texture and sensory attributes evolution during bread storage, and thus to optimise storage conditions and product formulation. This is because parameters of the model are actually product properties, that is, physical properties of the material. In this way, we could assess different product formulations and their evolution during

storage by relating some key ingredients (e.g. starch content, water content) with the material properties.

Another model intermediate between the two presented here has been tested. In this model, as the first one, the crust was assumed to be a membrane, but the water vapour and the dry air content are calculated, as in the model 2, using a diffusion equation. The total pressure was no longer equal to atmospheric pressure but equal to the sum of the partial pressure of dry air and water vapour. The results were strictly equal to those given by the first model (the curves were the same). This is due to the pressure staying constant in the product. The teaching of this model is that when the hypothesis of constant pressure is realistic, there is no need to complicate the model by computing the pressure for the sake of precision, because it involves another equation and additional flow terms.

Regarding the modelling of the crust, considering that model 2 gives the most realistic results, it is clear that the crust cannot be assumed to be a membrane through which the evaporation flows. Such a model leads to significantly different results from a model in which the crust is represented as a zone distinct from the crumb. Moreover, it does not allow the water equilibration phenomenon from the crumb to the crust to be represented. It is necessary to take the crust into account as a zone with its own characteristics.

Finally, the optimal model, that is to say the simplest model in its equations, without sacrificing to the accuracy of the physical phenomena repre-

sented, would be a simplification of the second model by imposing the total pressure equal to atmospheric pressure. The governing equation for the dry air content would be removed as well as the flow term in the water vapour equation. The dry air content would be calculated from algebraic equations. In this way, the crust would be considered a zone with its own characteristics. This would provide the simplest possible model, limiting the numerical problems and the computation time, and giving results strictly identical to those given by model 2.

5. Conclusion

This work has provided results on the water transfer occurring during bread staling and on the techniques of modelling water transfer in bread.

Concerning the transfer phenomena, the numerical results indicate that a 1 cm-thick bread slice lost 1.3 g over 10.2 days, with the crumb losing almost 1.8 g and the crust gaining 0.4 g. The missing 0.1 g is probably due to numerical errors. Thus, nearly 25 % of the water lost by the crumb was gained by the crust while the rest evaporated into the atmosphere. This water transfer from crumb to crust has already been shown experimentally (Besbes et al., 2014).

Regarding the modelling of these transfers, the comparison of the results given by the two models shows that it is not necessary to compute the transfer for each gas (here water vapour and dry air) by a governing equation with the terms of accumulation, diffusion, flow and a source term, when the total

pressure is known to be constant and equal to atmospheric pressure. It is simpler, and probably limits the numerical problems, to remove the governing equation for one of the gases, calculating its partial pressure by subtracting the partial pressure of the other gases from atmospheric pressure. Then, the content of this gas in the product is deduced. Moreover, the flow terms for the other gases disappear from the equations.

Other information provided by this study is that, for realistic results, the crust cannot be considered a membrane of negligible thickness and characterised by its water vapour permeability. The crust is a zone interacting with the crumb for the transfers and considering this crust to be only a Neumann boundary condition gives significantly different results.

References

Bechtel, W. G., Meisner, D. F., Bradley, W. B., 1953. The effect of the crust on the staling of bread. Cereal Chemistry 30, 160–168.

Besbes, E., 2012. Dynamique de l'eau dans les matrices céréalières : étude de l'effet des conditions de cuisson sur le rassissement du pain de mie. Ph.D. thesis, Université de Nantes.

Besbes, E., Jury, V., Monteau, J.-Y., Le Bail, A., 2013. Water vapor transport properties during staling of bread crumb and crust as affected by heating rate. Food Research International 50 (1), 10–19.

Besbes, E., Jury, V., Monteau, J.-Y., Le Bail, A., 2014. Effect of baking conditions and storage with crust on the moisture profile, local textural

properties and staling kinetics of pan bread. LWT - Food Science and Technology 58 (2), 658–666.

Datta, A., 2005. Modelling heat and mass transfer in food systems: current state and needs. In: Pagliarini, G., Rainieri, S. (Eds.), Heat and Mass Transfer in Food Processing - Eurotherm Seminar 77. Università degli Studi di Parma, Parma, pp. 3–8.

Datta, A. K., 2007a. Porous media approaches to studying simultaneous heat and mass transfer in food processes. I: Problem formulations. Journal of Food Engineering 80 (1), 80–95.

Datta, A. K., 2007b. Porous media approaches to studying simultaneous heat and mass transfer in food processes. II: Property data and representative results. Journal of Food Engineering 80 (1), 96–110.

Hug-Iten, S., Handschin, S., Conde-Petit, B., Escher, F., 1999. Changes in starch microstructure on baking and staling of wheat bread. LWT - Food Science and Technology 32 (5), 255–260.

Jury, V., 2007. Transferts couplés masse chaleur d'une matrice alvéolée. application à la décongélation-cuisson du pain précuit surgelé. Ph.D. thesis, Université de Nantes.

Ronda, F., Caballero, P. A., Quilez, J., Roos, Y. H., 2011. Staling of frozen partly and fully baked breads. Study of the combined effect of amylopectin recrystallization and water content on bread firmness. Journal of Cereal Science 53, 97–103.

Roussel, P., Chiron, H., 2002. Les pains français. Évolution, qualité, production. MAE Editeurs ERTI, Vesoul.

Thorvaldsson, K., Janestad, H., 1999. A model for simultaneous heat, water and vapour diffusion. Journal of Food Engineering 40, 167–172.

Whitaker, S., 1977. Simultaneous heat, mass, and momentum transfer in porous media: a theory of drying. Advances in Heat Transfer 13, 119–203.

Figure captions

Figure 1: Summary of assumptions of each model

Figure 2: Geometry and Mesh. a: 1st Model, b: 2nd Model. The results were taken at the points shown on the figure. Points represent different zones taken to analyse local profiles, i.e. core, crumb, interface crumb-crust, crust, surface

Figure 3: Comparison of experimental and computed water content profiles: D0 after 2 h, D3 after 3 days, D7 after 7 days and D10 after 10 days of staling

Figure 4: Local liquid water content variation

Figure 5: Water vapour content variation

Figure 6: Dry air variation

Figure 7: Evaporation flow variation

Figure 8: Pores water saturation variation

Figure 9: Overall water content variation in a 1 cm-thick bread slice

Figure 10: Pressure profiles along the line (0, 0) - (55, 55) at t = 10.2 days

Figure 11: Comparison of the liquid water content given by models 1 and 2

Figure 12: Comparison of the water vapour content given by models 1 and 2

Figure 13: Comparison of the dry air content given by models 1 and 2

Figure 14: Comparison of the evaporation ow given by models 1 and 2

Figure 15: Comparison of overall water content given by models 1 and 2

Table 1 : Models parameters

Physical constants		
D_{av}	(m^2 s^{-1})	2.34×10^{-5}
R	(J mol^{-1} K^{-1})	8.314 5
M_{vap}	(kg mol^{-1})	18.02×10^{-3}
M_{air}	(kg mol^{-1})	28.96×10^{-3}
ρ_{liq}	(kg m^{-3})	998.98
μ_g	(Pa.s)	1,72 × 10-5
Product constants		
D_{liq} [a]	(m^2 s^{-1})	1.34×10^{-10}
Φ_{crumb}		0.811
Φ_{crust}		0.750
C	(s m^{-2})	5×10^{-4}
$\rho_{app,s,crumb}$	(kg m^{-3})	192
$\rho_{app,s,crust}$	(kg m^{-3})	330
WVP	(kg m^{-1} s^{-1} Pa^{-1})	4.67×10^{-11}
e	(m)	0.005
Environmental parameters		
T	(°C)	15
P_{atm}	(Pa)	101 325
RH		0.9

[a] 1st model

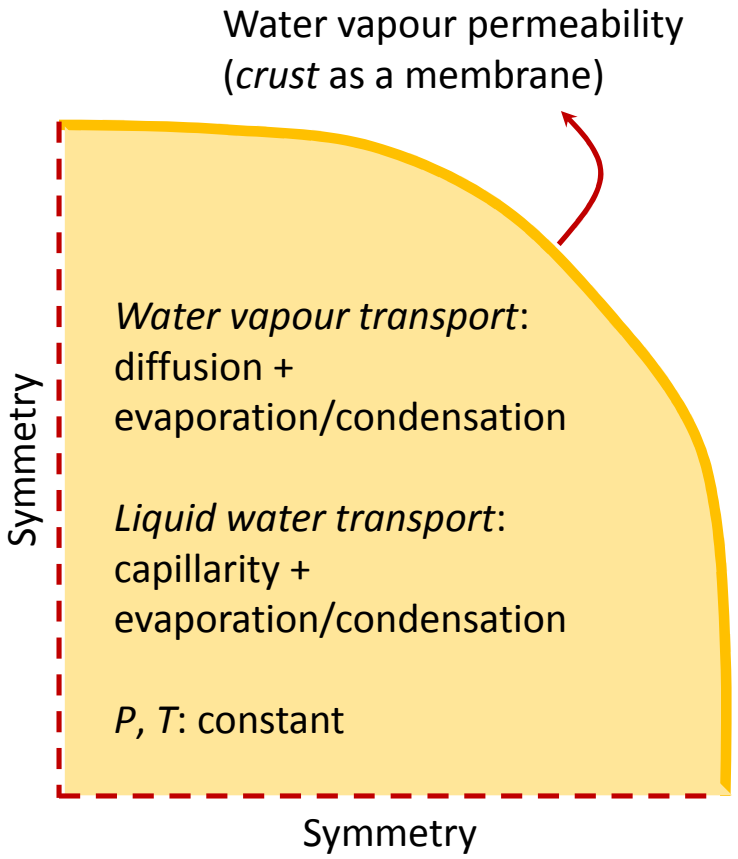

(a) Model 1

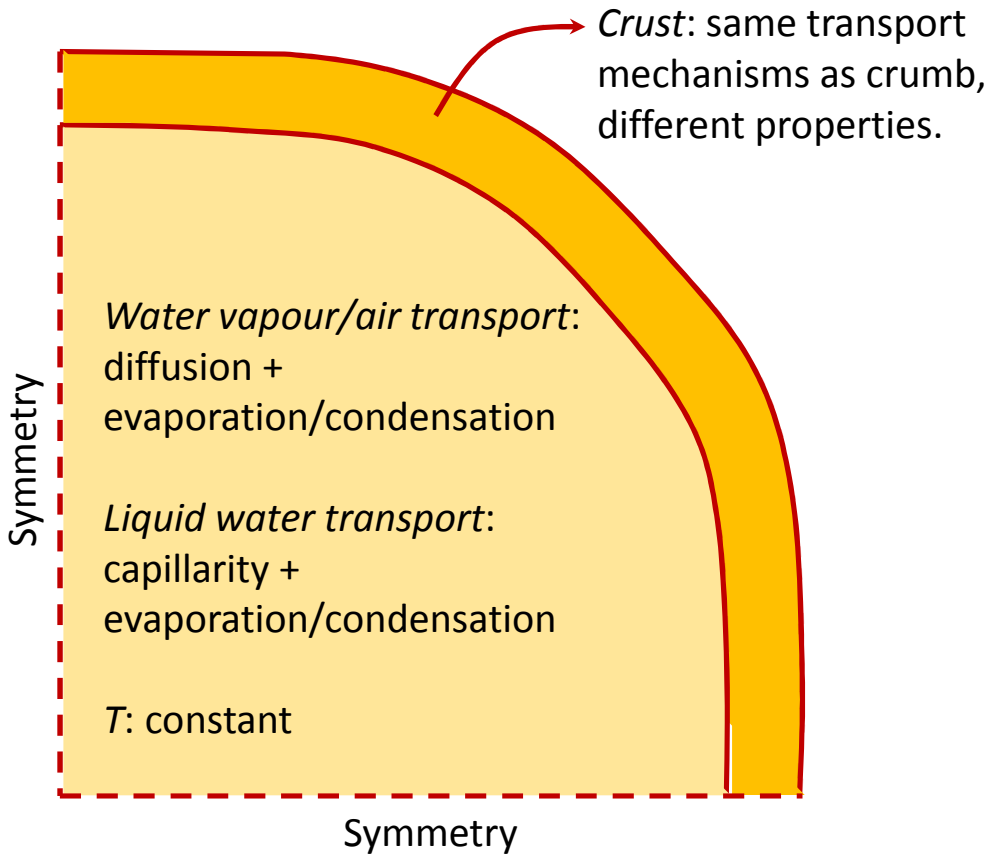

(b) Model 2

a

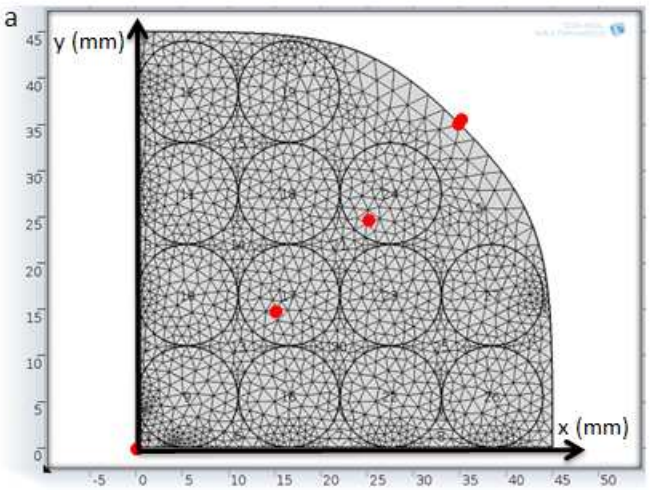

b

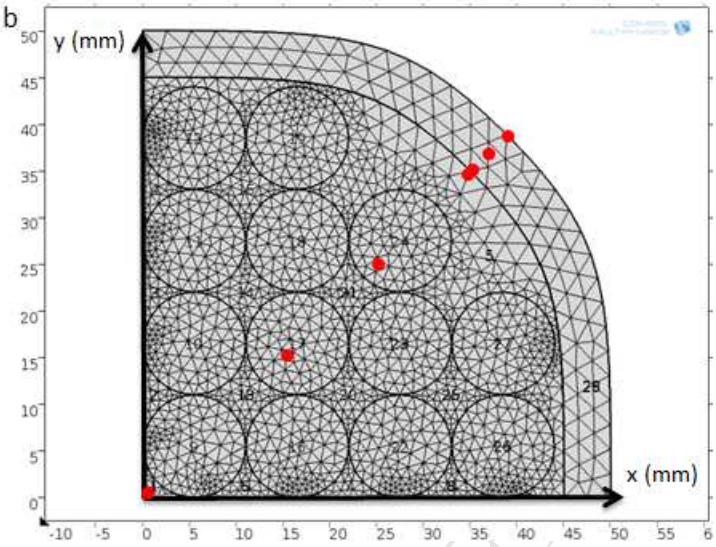

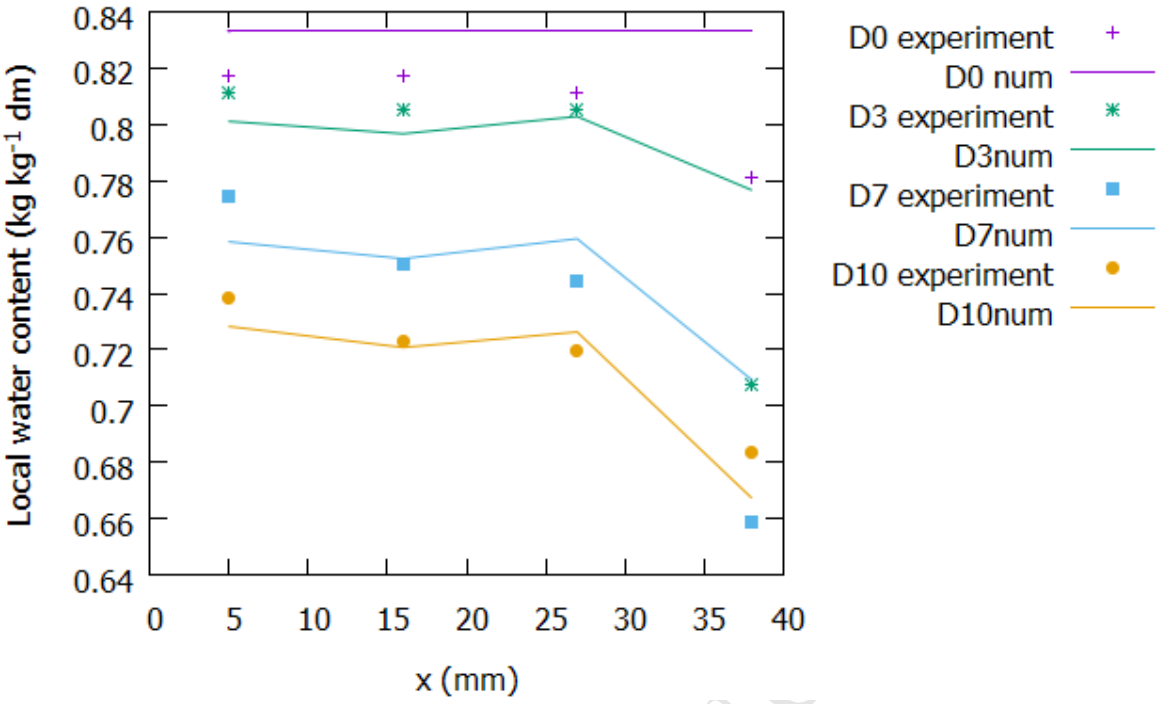

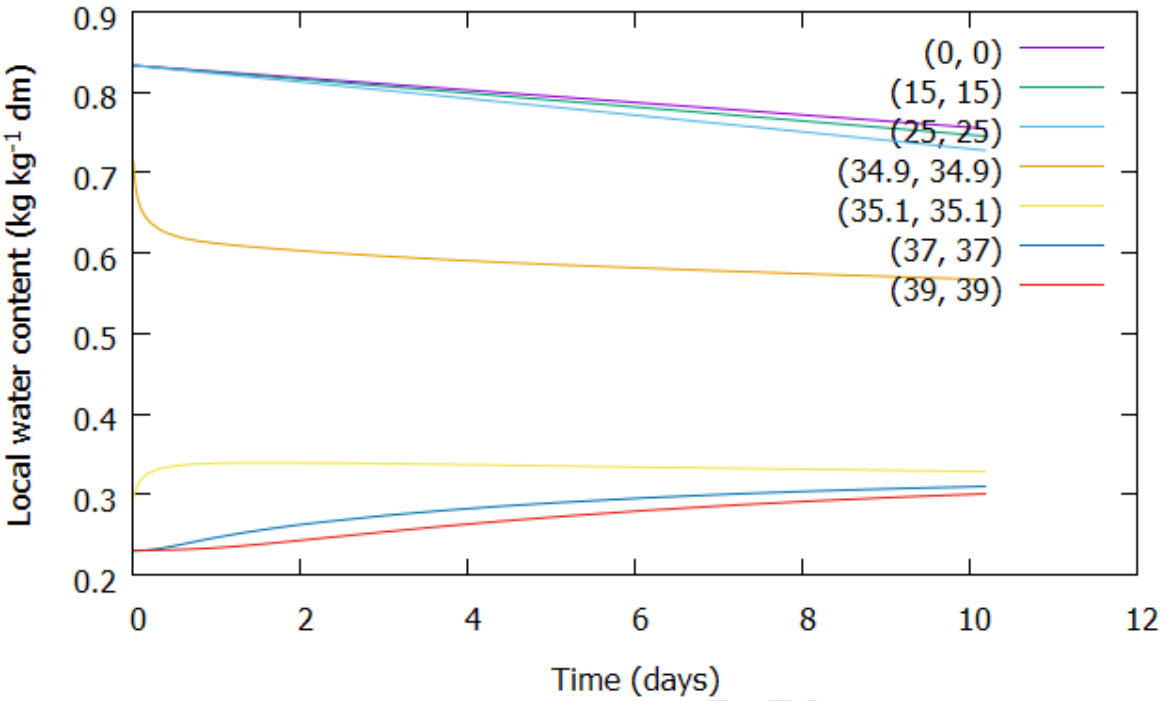

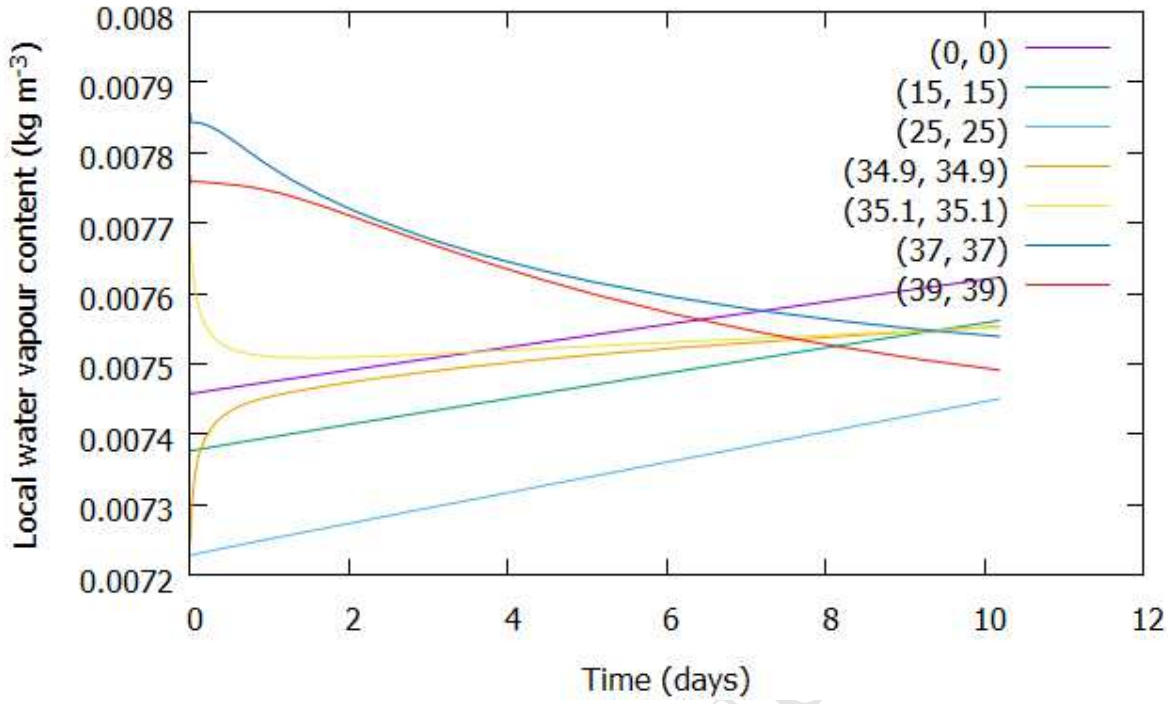

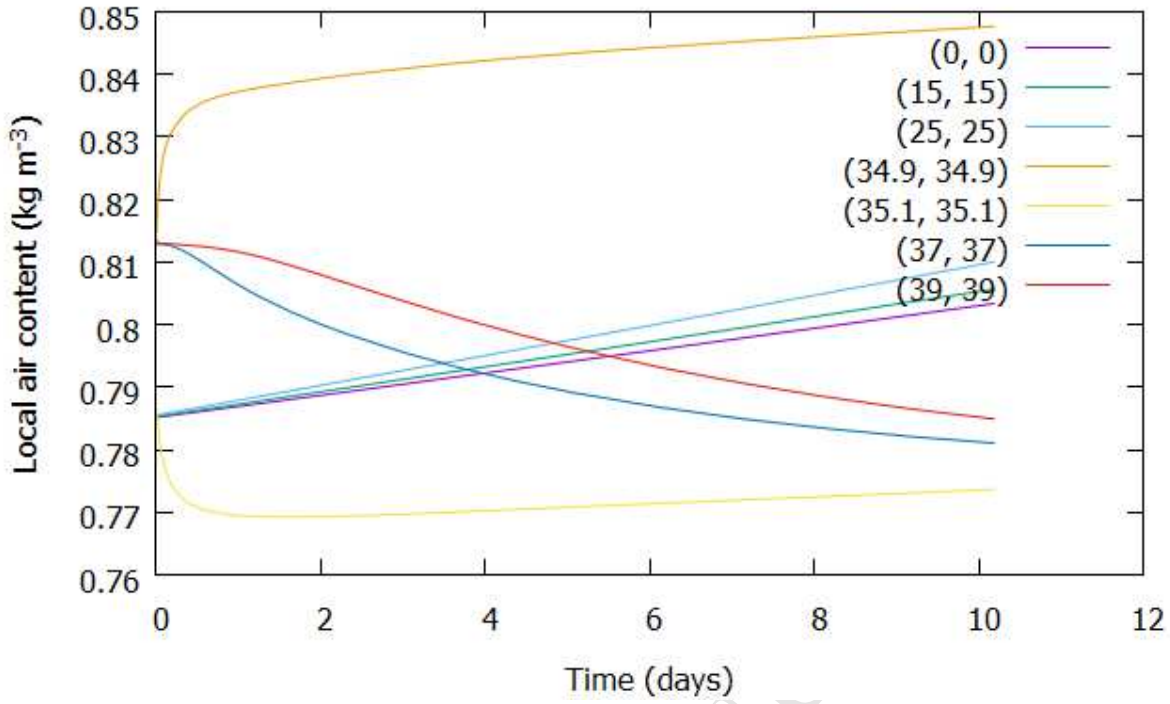

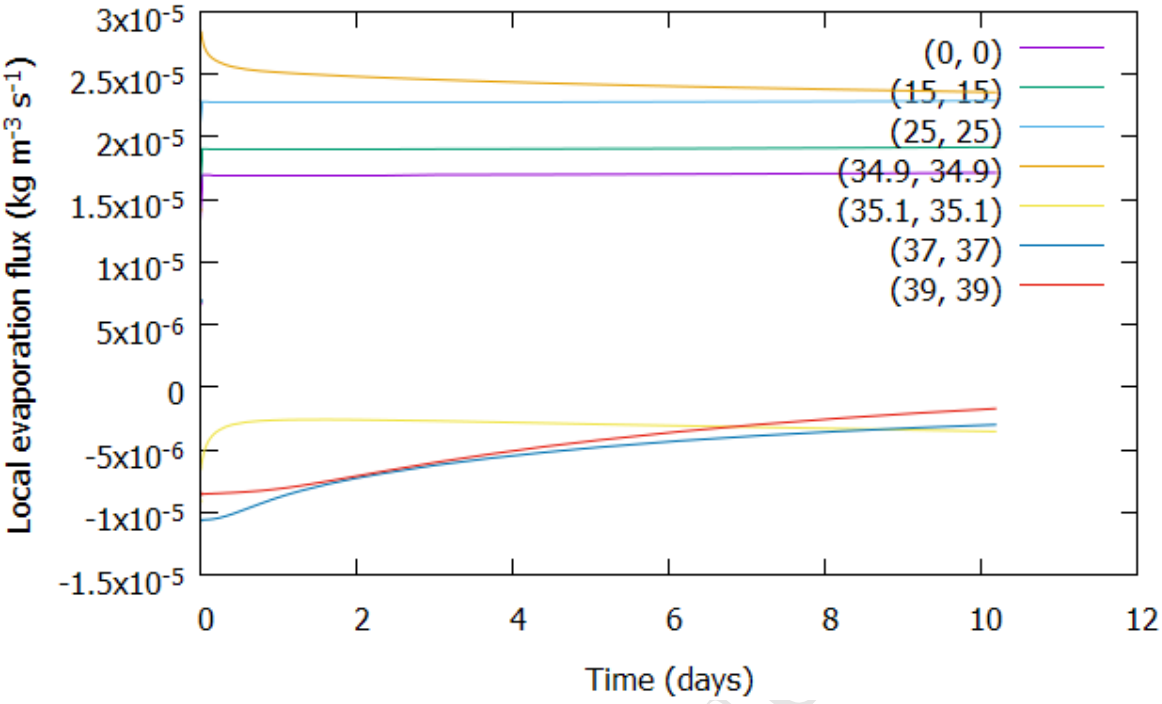

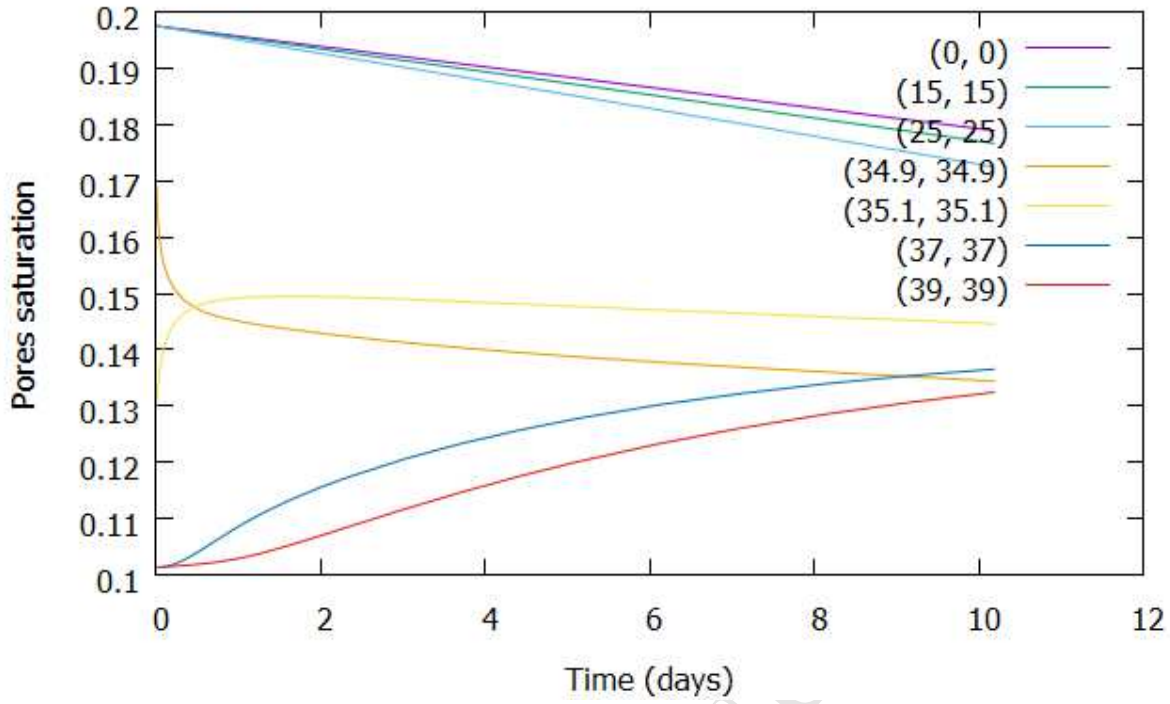

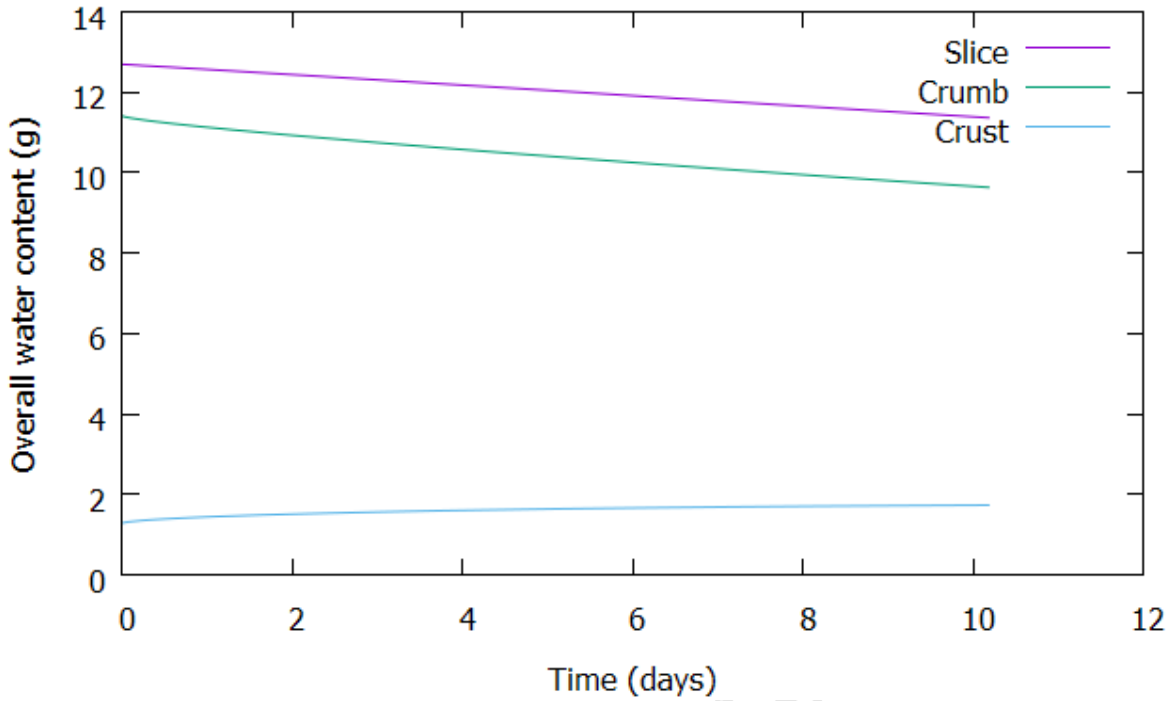

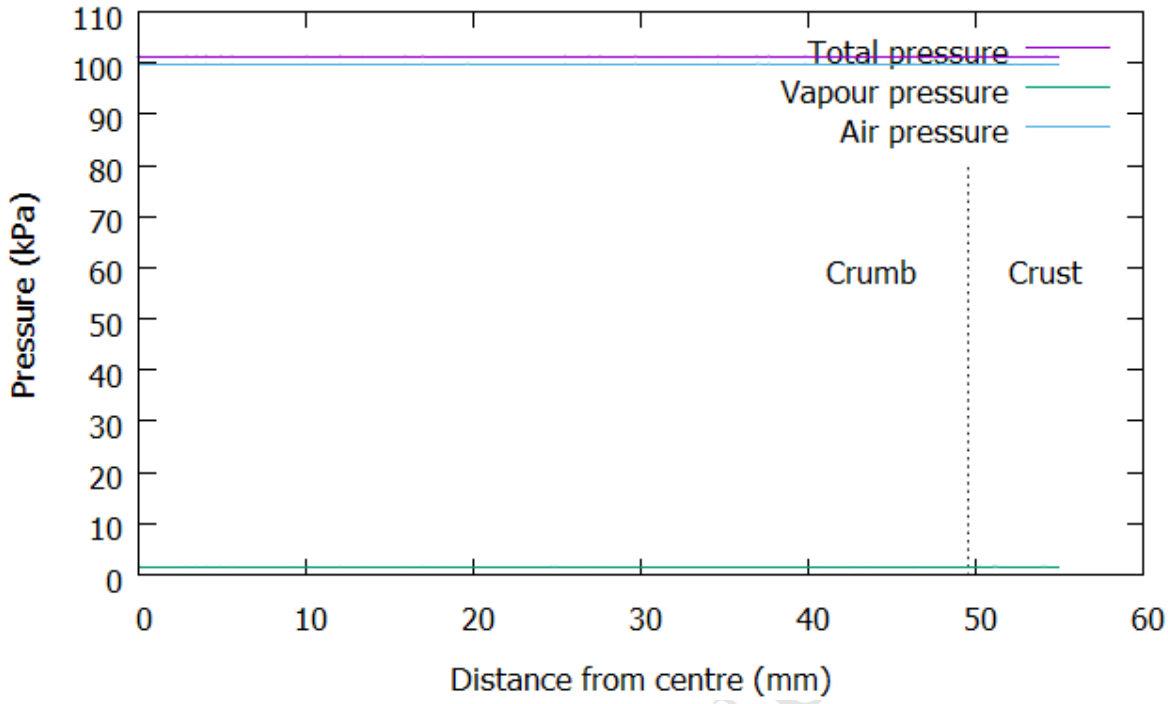

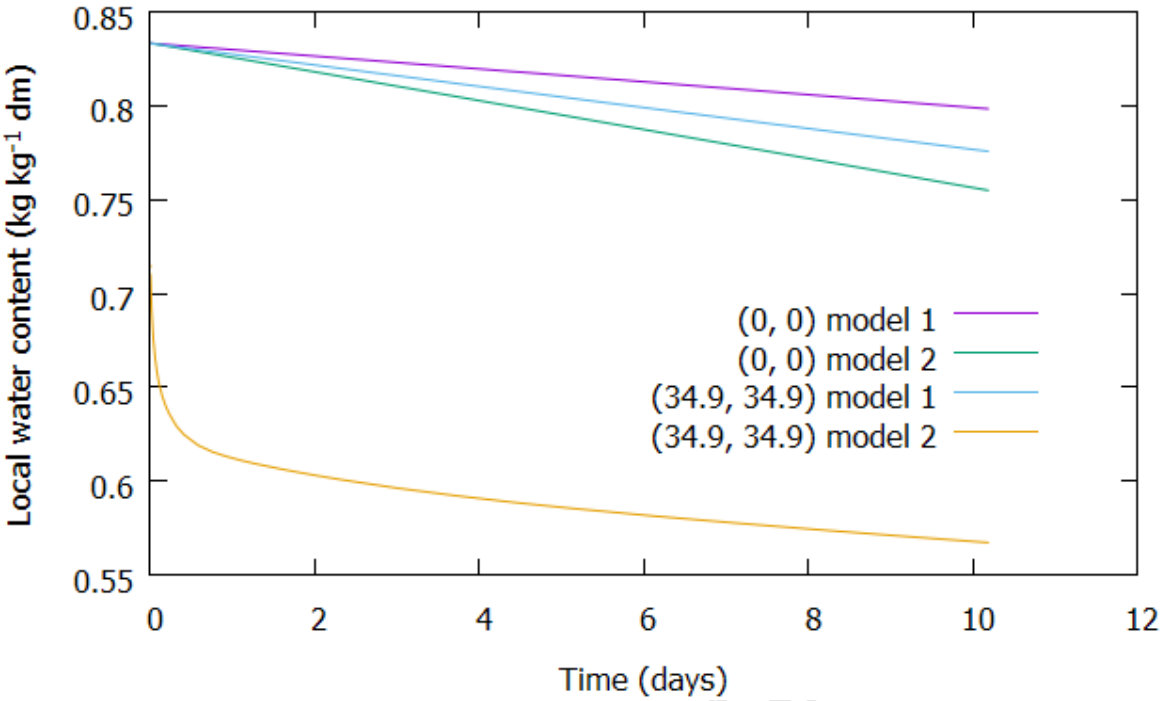

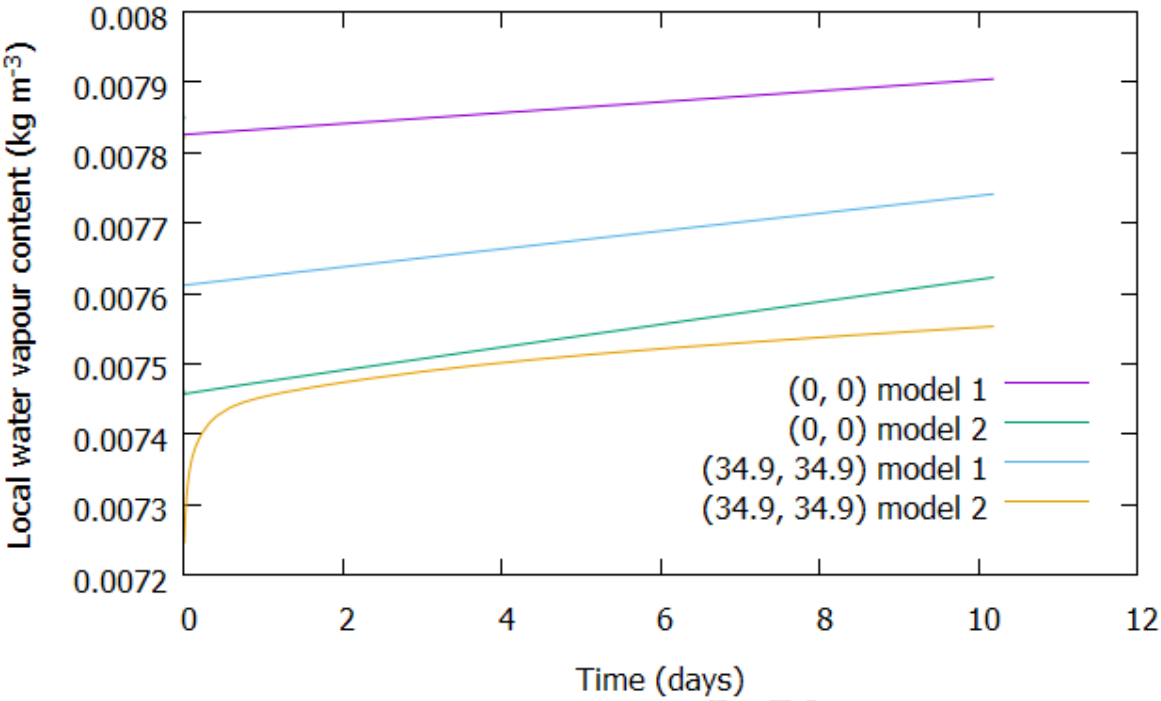

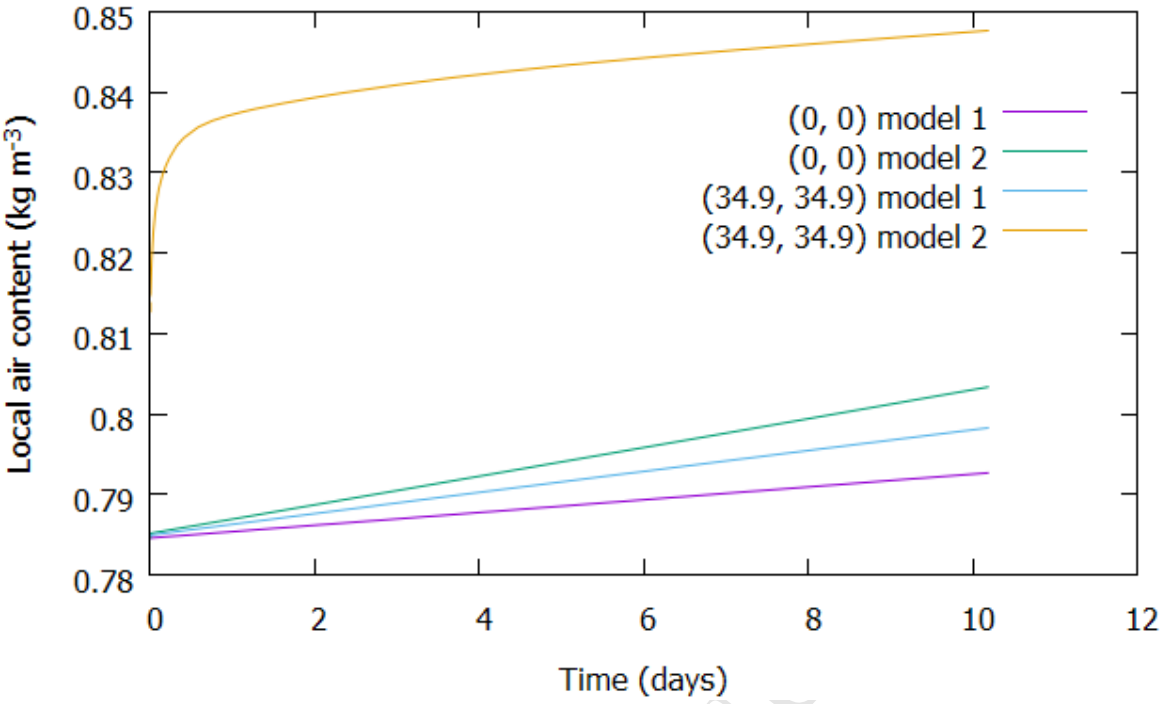

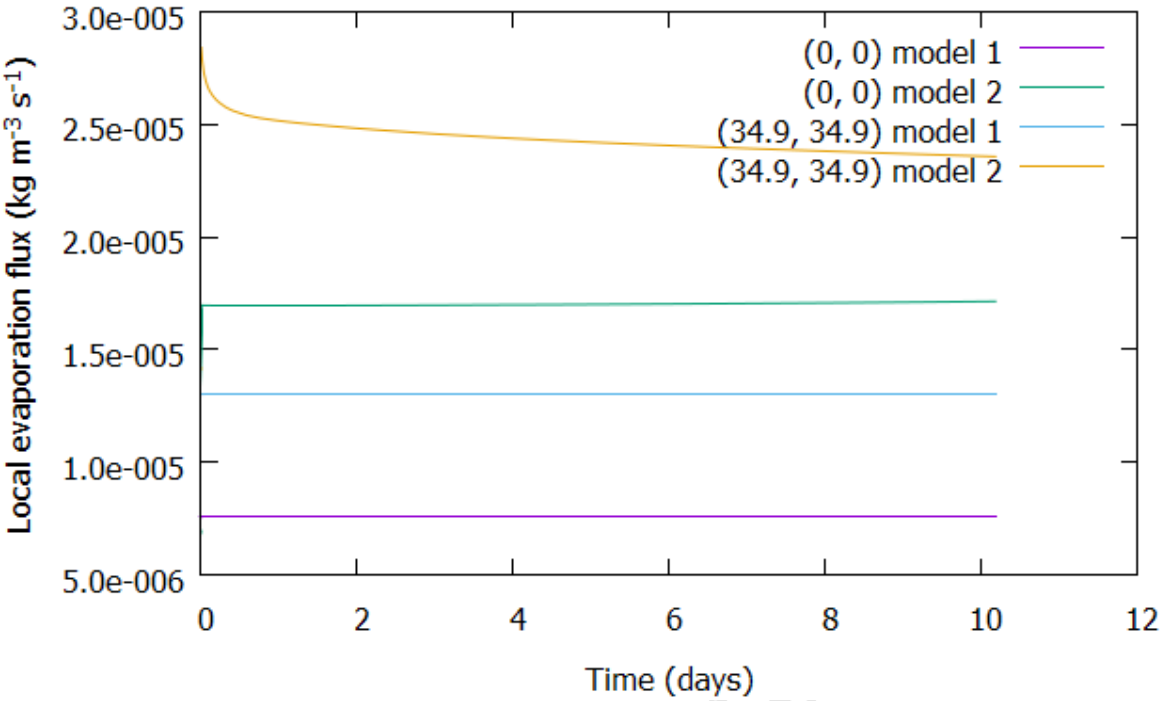

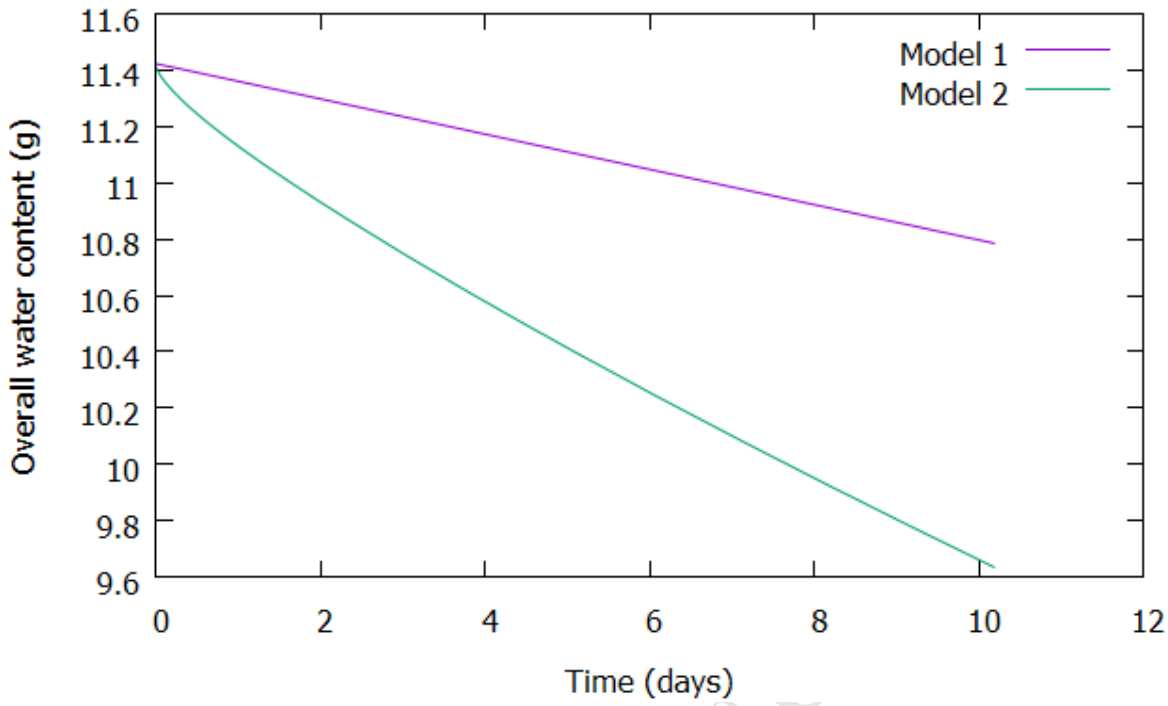

- Liquid water is transferred by capillary diffusion and water vapour migrates by molecular diffusion; Darcy's flow can be neglected.
- There is rebalancing of water from crumb to crust during staling.
- To model the water transfer, considering the crust as a membrane permeable to water vapour is not sufficient.
- Evaporation and condensation also take place during isothermal storage of bread.